

An accelerator scenario for a hard X-ray free electron laser combined with high energy electron radiography ^{*}

Tao Wei(魏涛)^{1,2;1)} Yiding Li(李一丁)¹ Guojun Yang(杨国君)¹ Jian Pang(庞健)¹

Yuhui Li(李煜辉)² Peng Li(李鹏)^{3,2} Joachim Pflueger² Xiaozhong He(何小中)¹

Yaxin Lu(卢亚鑫)¹ Ke Wang(王科)¹ Jidong Long(龙继东)¹ Linwen Zhang(章林文)¹ Qiang Wu(吴强)¹

¹ Institute of Fluid Physics, China Academy of Engineering Physics, P.O. Box 919-106, Mianyang 621900, China

² European XFEL GmbH, Hamburg 22607, Germany

³ Institute of Applied Electronics, China Academy of Engineering Physics, Mianyang 621900, China

Abstract: In order to study the dynamic response of the material and the physical mechanism of fluid dynamics, an accelerator scenario which can be applied to both hard X-ray free electron laser and high energy electron radiography is proposed. This accelerator is mainly composed of a 12 GeV linac, an undulator branch and an eRad beamline. In order to characterize a sample's dynamic behavior in situ and real-time with XFEL and eRad simultaneously, the linac should be capable of accelerating the two kinds of beam within the same operation mode. Combining in-vacuum and tapering techniques, the undulator branch can produce more than 10^{11} photons per pulse in 0.1% bandwidth at 42 keV. Finally, an eRad amplifying beamline with 1:10 ratio is proposed as an important complementary tool for the wider view field and density identification ability.

Keywords: XFEL, eRad, linac, undulator, emittance

PACS: 29.20.Ej, 29.27.Eg, 29.30.Dn **DOI:** 10.1088/1674-1137/40/8/088101

1 Introduction

In order to study the dynamic response of the material and the physical mechanism of fluid dynamics, it is suggested that there should be simultaneously three probe scales [1], the micro level, meso level and macro level, on which the detection of multi-spatial and multi-temporal phenomena can be made.

At macro scale, the high energy proton radiography [2,3] (pRad) technique is a capable diagnostic tool which can detect samples up to decimeter view field with a maximum resolution of tens of microns. Unfortunately, it is hard for pRad to achieve higher resolution even for thinner samples because of the beam quality of proton beams.

In comparison with proton beams, electron beams can easily obtain better quality because of less impact caused by the space charge effect. Thus high energy electron radiography [4] (eRad) could have better performance at meso scale, with the advantage of less emittance and energy spread. It is worth noting that eRad cannot replace pRad at macro scale because of the poor penetrating power.

At micro scale, X-ray free electron laser (XFEL) is a

unique diagnostic tool which can achieve resolution from micron to sub-nanometer [5].

2 Linac

In order to produce high brightness XFEL, an electron linear accelerator (linac) which acts as beam provider is indispensable. There is no doubt that such a linac can also provide beam for eRad. However the requirements for XFEL beams and eRad beams are quite different. The key point is to ensure the simultaneous acceleration of the two kinds of electron bunches within the same operation mode. Shown in Table 1 are the beam parameters for XFEL and eRad individually.

Shown in Fig. 1 is a sketch map of this accelerator. Two kinds of electron bunches, which are used for XFEL and eRad respectively, are produced by the injector. All of them are accelerated to 12 GeV energy at the end of the linac, and then they are separated into different branches. The XFEL bunches move along a sinusoidal trajectory under the periodic magnetic field from the undulator and emit coherent electromagnetic radiation which is called free electron laser. After shaping, focusing and monochromatization in the X-ray transport

Received 28 January 2016

^{*} Supported by China Academy of Engineering Physics (2014A0402016) and Institute of Fluid Physics (SFZ20140201)

1) E-mail: tao.wei@desy.de

©2016 Chinese Physical Society and the Institute of High Energy Physics of the Chinese Academy of Sciences and the Institute of Modern Physics of the Chinese Academy of Sciences and IOP Publishing Ltd

line, the XFEL eventually arrives at the sample. The eRad bunches are kicked into another branch, and after a longer trip they pass through the sample and produce a reversed image at the end of the eRad beamline.

Table 1. Parameters of XFEL beam and eRad beam at the end of a linac.

	XFEL electron bunch	eRad electron bunch
beam energy/GeV	12	12
bunch charge/nC	0.2	1
Rms bunch length/fs	22.5	230
peak current/kA	3	1.5
normalized slice emittance/ μm	0.25	1.08
Normalized emittance/ μm	0.32	1.1
energy spread (%)	0.015	0.2

The performance of both XFEL and eRad is directly dependent on the beam quality of the electron bunches as produced by the injector and preserved by the main linac. In order to acquire a sufficiently small emittance and energy spread, a photocathode injector with two drive laser system was proposed. The injector can provide two kinds of electron bunches (see Table 2).

Table 2. Parameters of XFEL beam and eRad beam at the end of the injector.

	XFEL electron bunch	eRad electron bunch
beam energy/MeV	150	150
bunch charge/nC	0.2	1
Rms bunch length/ps	2	3
peak current/A	30	100
normalized slice emittance/ μm	0.20	1.0
incoherent energy spread (%)	0.008	0.01

In order to reach SASE saturation in a reasonable length undulator, the designed XFEL electron beam should have a peak current of 3 kA. Such a high current density cannot be achieved directly by the injector under the premise of beam quality. Therefore the XFEL electron bunch is accelerated and compressed in a series of linacs (Linac-1, Linac-2 and Linac-3) and magnetic chicanes (BC-1 and BC-2) as shown in Fig. 1. Extensive simulation studies from Elegant [6] code indicate the beam quality is maintained very well.

The nominal linac design parameters for a 0.2 nC XFEL electron beam are summarized numerically in Table 3 and graphically in Fig. 2 below. Linac-1 is composed of three 3 m long S-band accelerating cavities ($f_{\text{rf}}=2.856$ GHz). It accelerates the XFEL electron bunch to 285 MeV with off-crest phase and generates energy-time correlation along the bunch as shown in Fig. 2(a). The energy-time correlation, which is generally called the energy chirp, is initially present when preparing for the bunch compression. A short high order harmonic cavity (0.6 m long, $f_{\text{rf}}=11.424$ GHz) is designed to remove the quadratic energy-time correlation. As shown in Fig. 2(b), Linac-X can cancel the rf curvature non-linearity generated in Linac-1; it operates at 180° and decelerates the bunch energy by 12 MeV.

The first bunch compressor [7] is a 4-dipole chicane (BC-1), which shortens the XFEL electron bunch to 260 fs rms. Due to the influence of coherent synchrotron radiation [8] (CSR) and the longitudinal space charge effect (LSC), the incoherent energy spread will increase as shown in Fig. 2(c). In fact, the parameter selection of a bunch compressor is always a compromise between beam quality and compression ratio. Linac-2 ($f_{\text{rf}}=2.856$ GHz) accelerates the bunch to 2.08 GeV, also at an off-crest phase, which maintains the desired linear energy chirp as shown in Fig. 2(d).

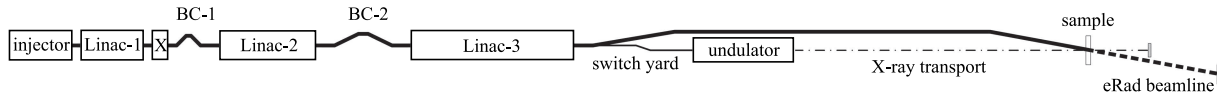


Fig. 1. Schematic diagram of an accelerator for simultaneous production of XFEL and eRad.

Table 3. Nominal linac parameters for 0.2 nC XFEL electron bunch.

	E_{in}/GeV	$E_{\text{out}}/\text{GeV}$	$\sigma_{t\text{-in}}/\text{ps}$	$\sigma_{t\text{-out}}/\text{ps}$	$\sigma_{\delta\text{-in}}(\%)$	$\sigma_{\delta\text{-out}}(\%)$	$\phi_{\text{rf}}(^{\circ})$	R_{56}/mm
Linac-1	0.15	0.28	2.0	2.0	0.01	1.1	-33.5	—
Linac-X	0.28	0.27	2.0	2.0	1.1	1.15	180	—
BC-1	0.27	0.27	2.0	0.26	1.15	1.15	—	-44.9
Linac-2	0.27	2.08	0.26	0.26	1.15	0.4	-37.5	—
BC-2	2.08	2.08	0.26	0.023	0.4	0.4	—	-17.9
Linac-3	2.08	12.18	0.023	0.023	0.4	0.015	+12	—

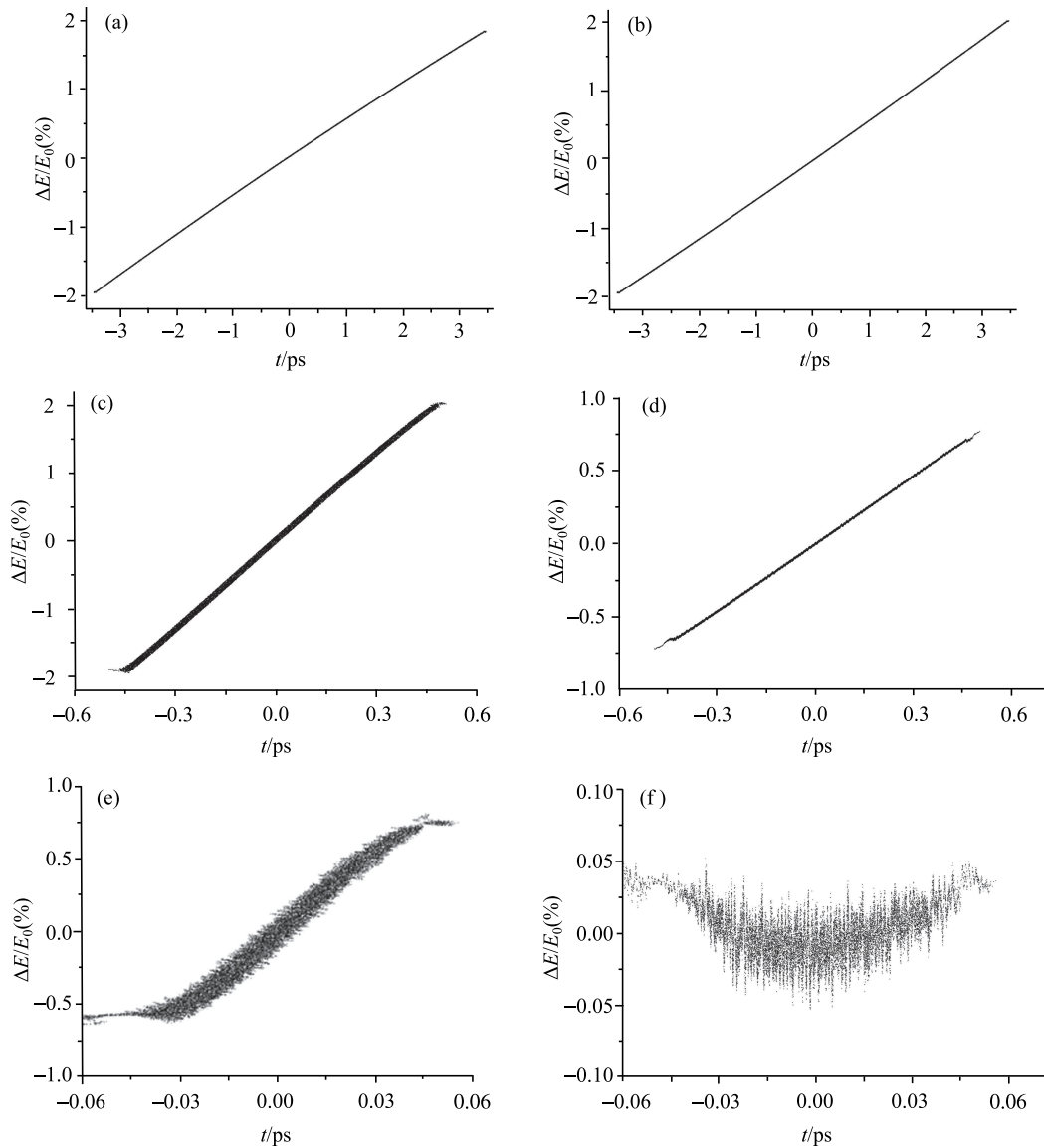


Fig. 2. The longitudinal phase space distribution of a 0.2 nC XFEL electron bunch after Linac-1 at 0.28 GeV (a), after Linac-X at 0.27 GeV (b), after BC-1 7.7 times compression section (c), after Linac-2 at 2.08 GeV (d), after BC-2 11 times compression section (e) and after Linac-3 at 12.17 GeV (f).

The second bunch compressor is another 4-dipole chicane (BC-2) which compresses the XFEL electron bunch to its final value of 22.5 fs as shown in Fig. 2(e). Finally, Linac-3 accelerates the bunch to 12 GeV, in which positive acceleration phase is chosen to cancel the time-correlated coherent energy spread.

Shown in Fig. 3 is the current distribution at the end of the linac. The very high peak current generated by the compression process can drive micro-bunching instability, which can damage both the slice emittance and the slice energy spread. In order to damp this effect, a laser-heater is placed in the injector section to adjust the initial incoherent energy spread. The simulation result shows

8×10^{-5} initial incoherent energy spread is sufficient to suppress the instability without adding too much energy spread at the entrance of the undulator.

All mentioned above are the longitudinal dynamics of a 0.2 nC XFEL electron bunch. In fact, the transverse dynamics are also necessary, especially for the beam emittance.

A FODO structure with betatron phase advance 60° per cell is chosen as the focusing lattice for Linac-1. Three acceleration cavities are located in 1.5 cells with equally spaced 0.4 m insert sections where 0.1 m quadrupole magnets and BPM-steering pairs can be arranged. A short X-band cavity is located in the following

drift. BC-1 is composed of four 0.2 m sector dipole magnets. It is an achromatic structure naturally and the dispersion function remains zero in the outer space. In order to weaken the CSR effect in the BC-1 section, the horizontal beta function (β_x) should be as small as possible, especially in the latter two dipoles when the bunch compression reaches the maximum value. As shown in Fig. 4, β_x is small enough in BC-1 and the emittance dilution due to the CSR effect is less than 10%.

A FODO structure with 60° phase advance per cell and 13 m period length is used in Linac-2. Every two cavities are connected together and placed between the quadrupole magnets as shown in Fig. 5.

The BC-2 compression section has nearly the same design constraints as BC-1 except for a stronger CSR effect. Moreover, the beam diagnostic sections are necessary at both ends. The emittance dilution can be controlled within 20% by selecting appropriate Twiss parameters as shown in Fig. 6.

Linac-3 adopts the FODO structure with 54° phase advance per cell and 25.2 m period length, as shown in

Fig. 7, every four cavities connected together and 168 cavities located in 21 cells. In order to provide enough focusing strength, the quadrupole magnets are up to 0.2 m long.

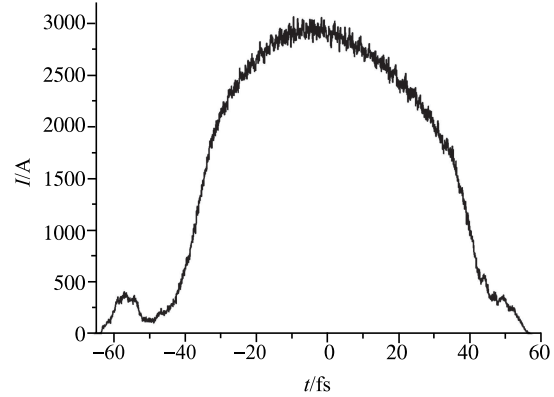


Fig. 3. The current distribution of a 0.2 nC XFEL electron bunch along the beam length at the end of the linac.

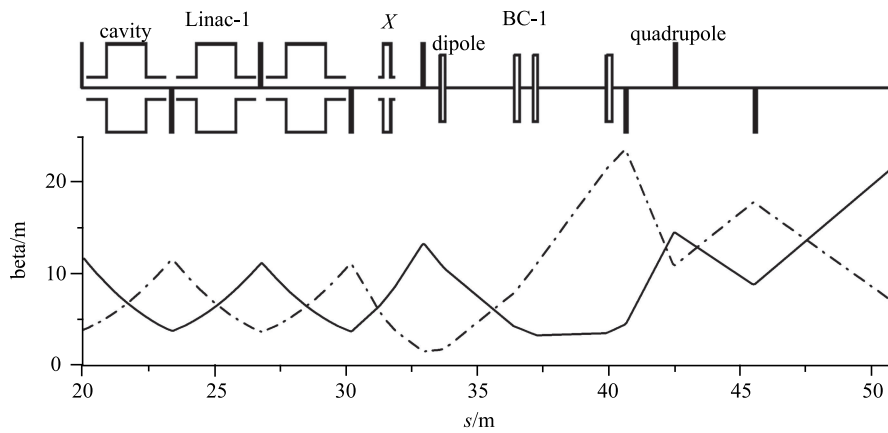


Fig. 4. Twiss parameters along Linac-1 and Linac-X ($S < 33$ m) and through the BC-1 chicane and emittance diagnostic section ($S > 41$ m). The solid line represents β_x and the dashed line represents β_y .

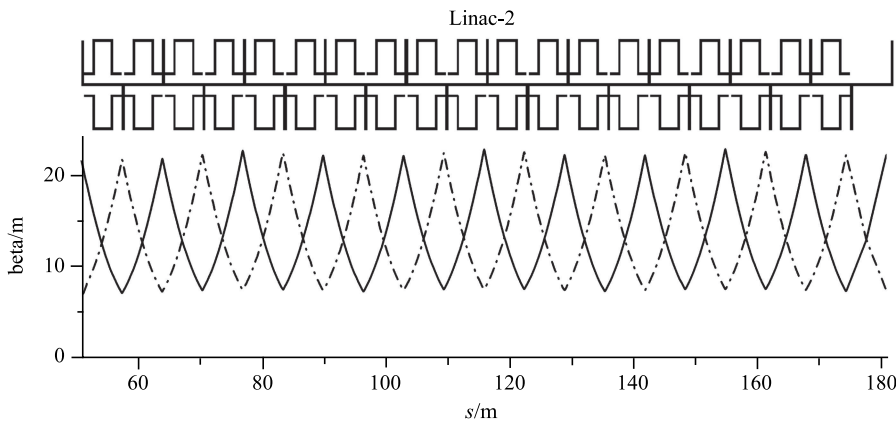


Fig. 5. Twiss parameters along Linac-2. The solid line represents β_x and the dashed line represents β_y .

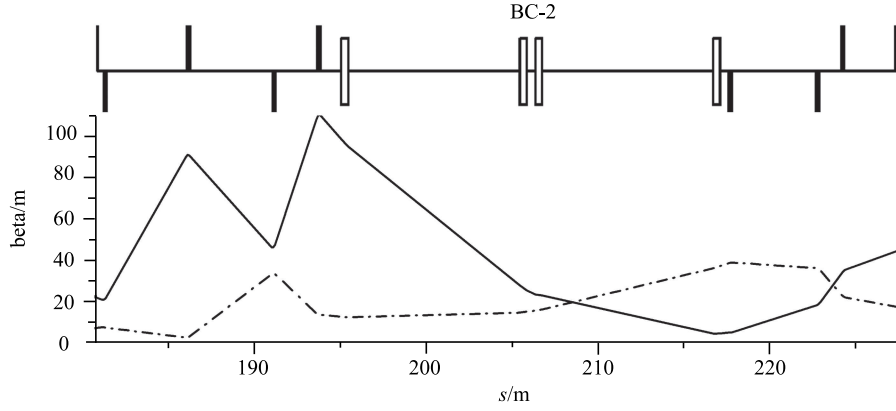


Fig. 6. Twiss parameters along the BC-2 chicane and beam diagnostic sections ($S < 194$ m and $S > 218$ m). The solid line represents β_x and the dashed line represents β_y .

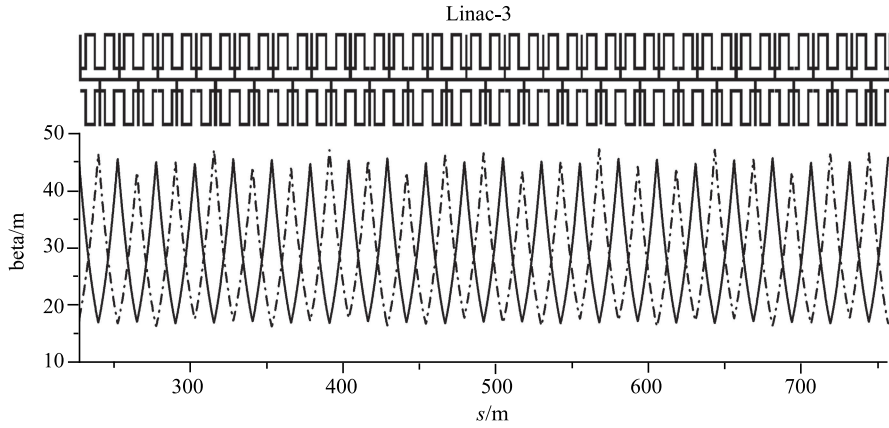


Fig. 7. Twiss parameters along Linac-3. The solid line represents β_x and the dashed line represents β_y .

All the parameters mentioned above are suitable for a 0.2 nC XFEL electron bunch, and the beam quality can satisfy the design guideline by means of these parameters. But these parameters are not sufficient for a 1 nC eRad electron bunch because it suffers much more serious instability than the XFEL bunch.

In order to achieve the simultaneous acceleration of two kinds of beam, all machine parameters remain unchanged except the initial phase of the eRad beam is delayed 10° which can be implemented by adjusting the

timing trigger of the injector laser system. As shown in Table 4, it is possible to completely change the linac parameters by varying only the initial acceleration phase. Comparing Table 3 and Table 4, the eRad electron bunch has a lower compression ratio and peak current, and the corresponding emittance dilution can be ignored. However, the coherent energy spread is hard to cancel totally. Even so, the beam quality of the eRad electron bunch is still within the specifications.

Table 4. Nominal linac parameters for a 1 nC eRad electron bunch.

	E_{in}/GeV	E_{out}/GeV	σ_{t-in}/ps	σ_{t-out}/ps	$\sigma_{\delta-in}(\%)$	$\sigma_{\delta-out}(\%)$	$\varphi_{rf}/(^{\circ})$	R_{56}/mm
Linac-1	0.15	0.3	3.0	3.0	0.02	1.16	-23.5	—
Linac-X	0.3	0.29	3.0	3.0	1.16	1.76	220	—
BC-1	0.29	0.29	3.0	0.64	1.76	1.76	—	-39.9
Linac-2	0.29	2.13	0.64	0.64	1.76	0.71	-35.85	—
BC-2	2.13	2.13	0.64	0.23	0.71	0.71	—	-17.2
Linac-3	2.13	12.23	0.23	0.23	0.71	0.19	+12.16	—

3 Undulator branch

The undulator branch is made up of 50 individual undulator [9] segments. Each segment has an in-vacuum permanent-magnet planar hybrid undulator with period length 18 mm and nominal gap 6 mm. The gap will be adjusted to yield effective undulator parameter K from 2.03 to 1.3. The permanent magnet is produced from rare-earth material $\text{Sm}_2\text{Co}_{17}$ with remanent field 1.1 Tesla. In order to provide good electrical boundaries, a 100 μm thick copper-nickel coated foil covers the magnets. Shown in Table 5 are the main parameters of the undulator magnet.

Table 5. The main parameters of the undulator magnet.

parameter	value	
type	hybrid, in-vacuum	
undulator period λ_u/mm	18	
remanent field B_r/T	1.1	
adjustable gap range/mm	3.5–6	
undulator parameter K	2.03	1.3
undulator gap/mm	3.5	6
peak field/T	1.2	0.77

The undulator branch adopts a FODO lattice, and only one undulator segment is placed between two focusing quadrupoles. Such a short betatron period structure is advantageous in reducing the beam size. In order to achieve ultra-hard 42 keV XFEL radiation with relatively low energy electron beam, an in-vacuum undulator is used. More detailed parameters are listed in Table 6.

Generally the tapering technique increases photon yield sharply because of the energy-loss compensation along the undulator, but it increases the undulator branch length and cost at the same time. Shown in Fig. 8 are the results from GENESIS [10] simulation, combining in-vacuum and tapering techniques. It is clear that a 200 m undulator length is a good choice.

4 eRad beamline

The high energy electron radiography technique depends on the use of a particular amplifying magnetic lens to compensate for the small angle multiple Coulomb scattering (MCS) that occurs as energetic electrons pass through the sample. The use of such a magnetic lens turns the otherwise troubling complications of MCS into an asset. Electrons undergo the combined processes of small angle Coulomb scattering and ionization energy loss, each with its own unique dependence on material properties. These effects make possible the simultaneous determination of both material amounts and material identification.

Table 6. Parameters of the undulator branch.

parameter	value
beam energy/GeV	12
RMS normalized slice emittance/ μm	0.25
RMS energy spread (%)	0.015
beam peak current/kA	3
RMS beam length/fs	23
undulator period λ_u/mm	18
undulator parameter K	1.3
nominal undulator gap/mm	6
undulator segment length/m	3.456
number of segments	50
focusing method	FODO
supercell length/m	8.064
branch length/m	201.6
betatron phase advance per cell	60°
average beta function/m	7.64
radiation wavelength/nm	0.03
photon energy/keV	42
average radiation power/GW	21
bandwidth (%)	0.08
photons per pulse	2.1×10^{11}

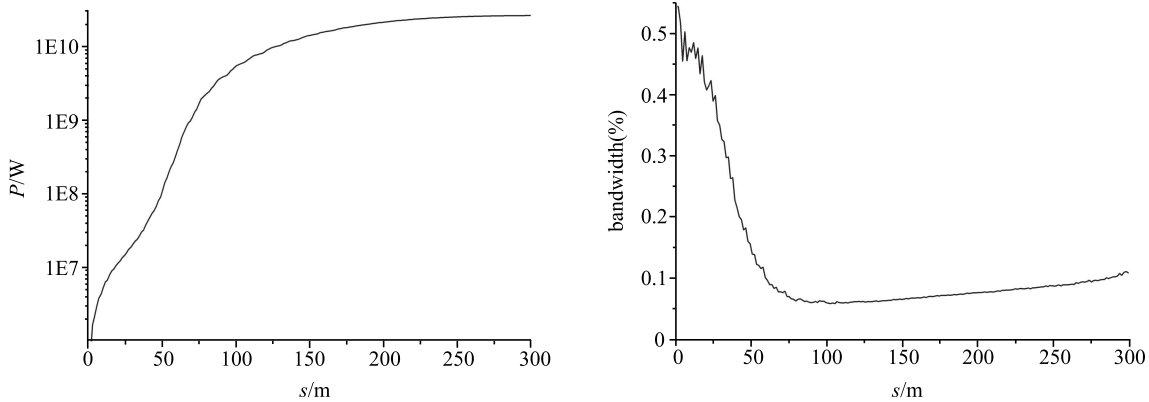


Fig. 8. Radiation power (left) and bandwidth (right) along undulator branch.

eRad requires a high energy beam to penetrate the sample while keeping the deflection angle and energy loss small enough to allow good spatial resolution. To improve the resolution, the image blur should be small as possible. It is typically dominated by chromatic aberrations due to energy spread of the injected beam in combination with the spread of energy loss after passing through the sample. The image blur can be expressed as

$$\Delta x = T_{126}\theta\delta/M, \quad (1)$$

in which θ is the deflection angle, mainly due to multiple Coulomb scattering (MCS), $\delta = \Delta E/E_0$ is the relative energy deviation, E_0 is the energy of a reference particle, T_{126} (for the x direction) and T_{346} (for the y direction) represent the second order chromatic aberration coefficients, which are decided by the lens system, and M is the image amplifying ratio.

The 1 nC eRad electron bunch travels a long trip (~ 1 km) in a separate branch adjacent to the XFEL before reaching the sample. At the same time, the transverse beam size expands 5–6 times by increasing the beta function to 1000 m. This can help illuminate the ~ 1 mm view field and decrease the image blur

caused by the insufficient transverse modulation of the beam [11]. In the case of the eRad bunch described in Table 1, the rms effective deflection angle due to insufficient transverse modulation is equal to $\sqrt{\varepsilon/\beta} = 0.22\mu\text{rad}$.

Shown in Fig. 9 is the schematic of the 12 GeV eRad beamline and its Twiss parameters. The total length is about 50 m, and the second order chromatic aberration coefficients T_{126} and T_{346} are 107 m and 59 m respectively.

Shown in Fig. 10 are the simulation results by Monte Carlo code GEANT4 [12]. In the simulation, we chose a copper sample 0.1 mm long. The rms plane projection deflection angle is $117\mu\text{rad}$, and the average energy loss is about 0.12 MeV, which leads to 1×10^{-5} additional energy spread. In contrast, ionization energy loss can be ignored for the much bigger incident beam energy spread 0.2%. Therefore, the image blur can be calculated as $2.5\mu\text{m}$ for the x direction and $1.4\mu\text{m}$ for the y direction. In fact, the angle sort function can be carried out by the collimator on the Fourier plane, electrons with greater angles can be cut off and higher resolution ability can be achieved.

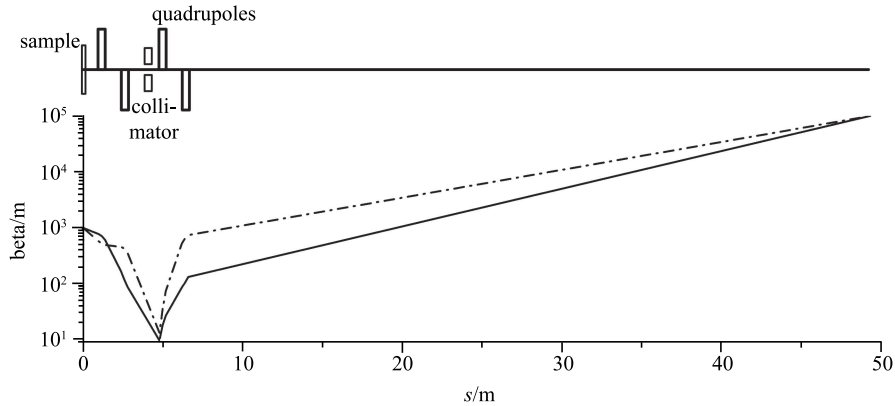


Fig. 9. Schematic of 12 GeV eRad beamline and its Twiss parameters (when $M=10$). The solid line represents β_x and the dashed line represents β_y .

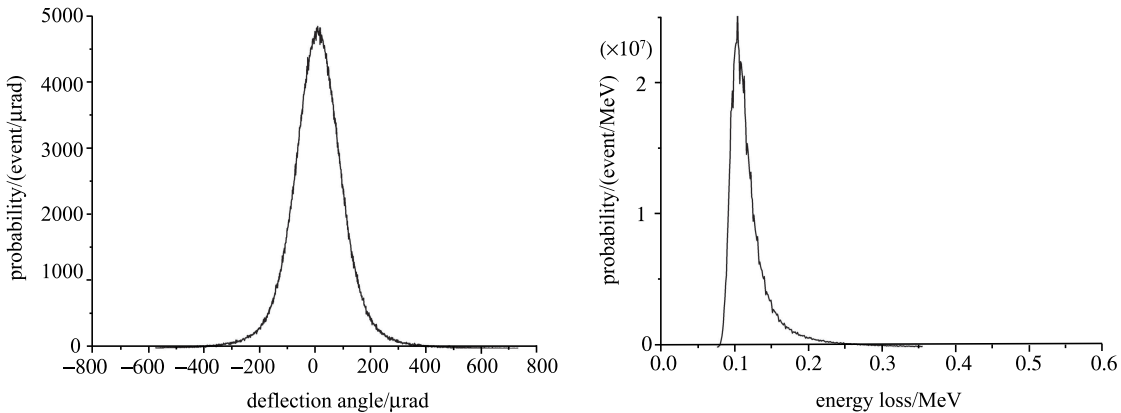


Fig. 10. The distribution of deflection angle and energy loss simulated by Geant4 when a 12 GeV electron beam passes through a 0.1 mm long copper sample.

5 Discussion and conclusions

In the normal conductive accelerator scenario described in this article, the XFEL electron beam and eRad electron beam can be accelerated within the same operation mode. All machine parameters remain unchanged except the timing trigger of the injector laser system, which can easily be achieved online. As the two kinds of electron bunches undergo different branches after the linac and the optical path difference is tens of nanoseconds, it is possible to separate them in the switch yard by kicker and septum magnet.

The transverse emittance of the XFEL electron beam plays a key role in the photon yield. Shown in Fig. 11 are the time-dependent simulation results by GENESIS. Normalized slice emittance of $0.3 \mu\text{m}$ is the minimum requirement. Apart from the CSR and space charge effect mentioned above, the influence of wake field on the transverse emittance cannot be ignored.

The imaging principle of high energy eRad originates in high energy proton radiography, but has yet to be put into practice in a specific implementation. The purpose of the amplifying beamline is to reduce the impact of point spread function (PSF) in the scintillator screen. The improvement of incident beam energy spread can

further upgrade the spatial resolution of eRad, especially for a relatively thin sample.

Dynamics studies require multiple pulses, which have not been mentioned in this article. To achieve high enough beam quality for multiple pulse XFEL electron bunches and eRad electron bunches, research is under way on beam quality degradation caused by wake field and beam loading.

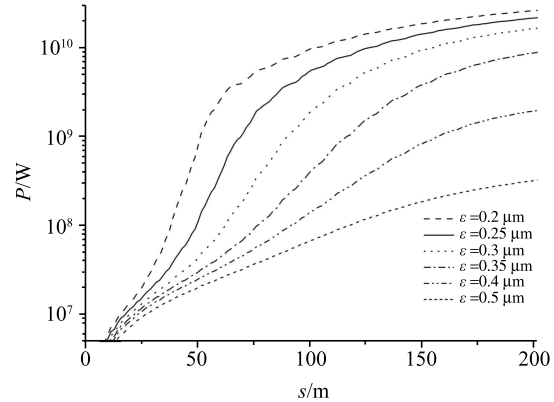


Fig. 11. The radiation power of 42 keV photons along the undulator for different normalized emittance.

References

- 1 J Sarrao et al, MaRIE 1.0: A flagship facility for predicting and controlling materials in dynamic extremes, LA-UR-12-00500
- 2 C L Morris, E. Ables, K.R. Alrick et al, Journal of Applied Physics, 2011, **109**: 104905
- 3 C L Morris, N.S.P king, K. Kwiatkowski et al, Reports on Progress in Physics, 2013, **76**: 046301
- 4 Frank Merrill, Frank Harmon, Alan Hunt et al, Nuclear Instruments and Methods in Physics Research B, 2007, **261**: 382–386
- 5 Richard Neutze, Phil. Trans. R. Soc. B, 2014, **369**: 20130318
- 6 Michael Borland, User's manual for elegant, http://www.aps.anl.gov/Accelerator_Systems_Division/Accelerator_Operations_Physics/manuals/elegant_latest/elegant.pdf
- 7 R. Li, Nuclear Instruments and Methods in Physics Research A, 1999, **429**: 310–314
- 8 K. Bane, Y. Ding, P. Emma et al, Measurements of Compression and Emittance Growth after the First LCLS Bunch Compressor Chicane, in Proceedings of PAC07 (New Mexico, USA)
- 9 T. Tanaka, T. Hara, R. Tsuru et al, In-vacuum Undulators, in Proceedings of the 27th international free electron laser conference (California, USA, 2005)
- 10 S. Reiche, Update on the FEL Code Genesis1.3, in Proceedings of FEL2014 (Basel, Switzerland)
- 11 Wei Tao, Yang Guojun, Long Jidong et al, Chinese Physics C, 2013, **37**(6): 068201
- 12 S. Agostinelli, J.Allison, K. Amako et al, Nuclear Instruments and Methods in Physics Research A, 2003, **506**: 250–303